KLEAR ENABLES PRE-TRANSPLANT FORECASTING OF ACUTE REJECTION IN DECEASED-DONOR KIDNEY TRANSPLANT RECIPIENTS

Anonymous authors
Paper under double-blind review

ABSTRACT

Kidney transplantation remains the gold standard for treating end-stage renal disease, yet acute T cell-mediated rejection (TCMR) and antibody-mediated rejection (ABMR) significantly compromise early graft outcomes and long-term survival. Current risk assessment relies on low-resolution Human Leukocyte Antigen (HLA) matching, which fails to capture the molecular nuances of the donor-recipient immune interface. This submission introduces KLEAR (Kidney Likelihood Estimator for Acute Rejection), a machine learning framework designed for pre-transplant risk stratification. KLEAR leverages high-resolution HLA typing to derive novel molecular features (E3-MoFs) capturing physiochemical mismatches. To address the challenges of high-dimensional tabular clinical data and severe class imbalance, we propose a two-stage methodology: first, a generative oversampling strategy using a Variational Autoencoder integrated with a Bayesian Gaussian Mixture Model (VAE-GMM) to align the latent manifolds of rejection phenotypes; and second, a hybrid architecture that feeds tree-based leaf embeddings from eXtreme Gradient Boosting (XGBoost) into a dense neural network (DNN). Using a multi-site cohort of 2,013 patients from Mayo Clinic, the largest integrated transplant provider in the United States, KLEAR was trained and validated in a pilot prospective study. KLEAR demonstrates a 5.0-fold increase in AUPRC for TCMR and a 7.5-fold increase for ABMR compared to random classifiers. A small prospective pilot cohort provides feasibility evidence, but its event count is too limited to support deployment claims. Overall, this study highlights how molecular features of HLA mismatches, combined with clinical variables, can improve prediction of TCMR and ABMR and proposes a novel modeling framework for pre-transplant risk stratification. Once further validated in a large-scale, multi-center, prospective study, KLEAR may potentially inform clinical decision-making and support trial enrichment in transplantation.

1 INTRODUCTION

The field of solid organ transplantation is currently navigating a period of unprecedented growth, with record-breaking volumes of deceased-donor kidney transplants being performed annually (WHO, 2025). Despite these procedural advances, the biological barrier of acute allograft rejection remains a primary determinant of graft longevity and patient quality of life (Hariharan et al., 2022). T cell-mediated rejection (TCMR) and antibody-mediated rejection (ABMR) occur in approximately 8–15% of recipients within the first year, leading to chronic injury, sensitization, and eventual graft failure (OPTN, 2023). The ability to accurately predict these events prior to transplantation is of paramount clinical importance, as it governs critical decisions regarding organ acceptance, induction immunosuppression intensity, and post-transplant surveillance frequency (Stegall et al., 2016; Vincenti et al., 2016; Kaplan et al., 2003; He et al., 2009; Mubarak et al., 2023; Menon et al., 2017).

Existing predictive models in the transplant domain, most notably the iBox system, have gained international recognition for their ability to forecast long-term graft loss (Klein et al., 2023; Loupy et al., 2019a). However, these systems are fundamentally reactive, relying on post-transplant data such as histology, proteinuria, and the presence of donor-specific antibodies (DSA) (Jucaud et al.,

Reviewers: please read the Reviewer Guidelines (iclr.cc/Conferences/2027/ReviewerGuidelines) and the AI Policy for Reviewers (iclr.cc/Conferences/2027/AIPolicyForReviewers). If you used AI to expand, edit, or polish your review, please provide the input text to the LLM. Better still, consider skipping the LLM and submitting your original text: we, and the authors, are much more interested in your unedited thoughts than in what an LLM has to say. AI-assisted or not, you are putting your name and reputation behind your review: LLM-generated falsehoods, hallucinations or misrepresentations are subject to disciplinary action, which may include desk-rejecting all papers you have authored.

2020; 2019). There remains a critical void in pre-transplant predictive tools that can integrate donor-recipient clinical characteristics (DRCs) with the complex immunogenetic landscape of Human Leukocyte Antigen (HLA) mismatches (Demir et al., 2025; Santos et al., 2024; Bezstarosti & Heidt, 2025b; Puttarajappa et al., 2025).

Traditional HLA matching utilizes antigen-level or low-resolution typing, which treats broad categories of HLA alleles as identical (Chou-Wu et al., 2025). This abstraction overlooks the fine-grained molecular differences, including variations in amino acid sequence, electrostatic charge, and hydrophobicity, that serve as the primary triggers for the recipient's immune system (OPTN, 2023; Hariharan et al., 2022). While high-resolution HLA typing is seeing broader clinical adoption at centers such as the Mayo Clinic, the integration of this high-dimensional molecular data into actionable risk scores is hindered by the limitations of standard statistical methods (Demir et al., 2025; Santos et al., 2024; Bezstarosti & Heidt, 2025b).

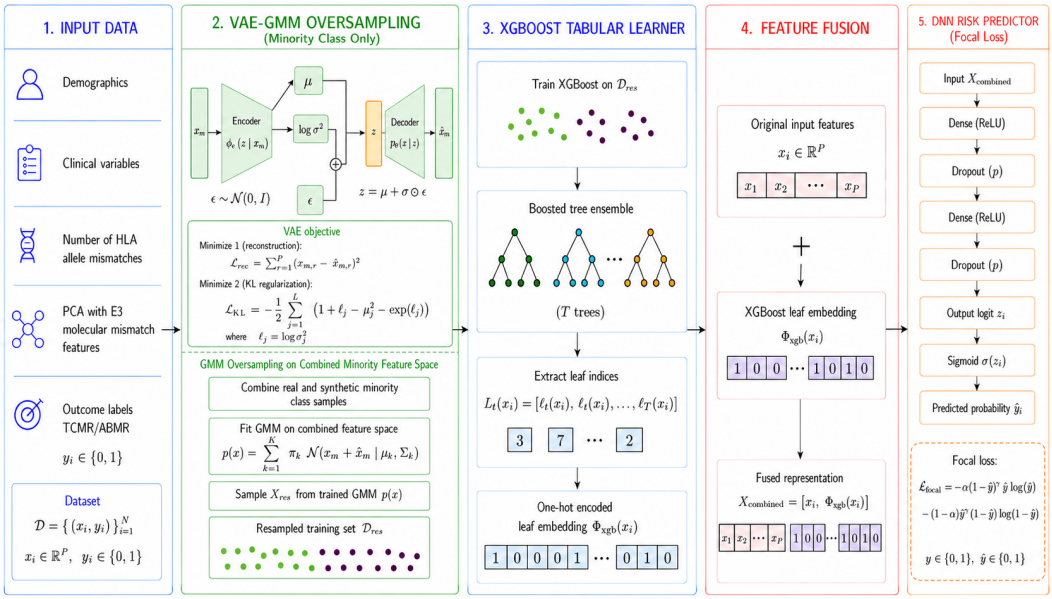

Figure 1: Overview of the KLEAR modeling pipeline. The pipeline takes donor-recipient clinical variables, HLA allele mismatch counts, PCA-reduced E3 molecular mismatch features, and outcome labels as input; applies fold-wise preprocessing and VAE-GMM oversampling; trains an XGBoost tabular learner; extracts tree leaf embeddings; fuses original and leaf-embedding features; and trains a dense neural network with focal loss to predict rejection probability.

In this submission, we present KLEAR (Kidney likelihood estimate for Acute Rejection), a hybrid machine learning framework that formalizes allograft rejection as a counterfactual risk estimation problem, as shown in Figure 1. KLEAR introduces several methodological innovations tailored to the nuances of clinical tabular data. First, we employ the E3 framework to quantify 95 molecular features of HLA mismatches (E3-MoFs), specifically tailored to the divergent pathways of TCMR and ABMR (Jordan et al., 2015; Loupy et al., 2019b; Gonzales et al., 2016). Second, we address the inherent class imbalance of rejection outcomes through a generative oversampling strategy that combines Variational Autoencoders (VAEs) with Gaussian Mixture Models (GMMs) to capture the multimodal distribution of high-risk patients. Finally, we utilize a hybrid modeling architecture where XGBoost-derived leaf indices are used as feature embeddings for a dense neural network, capturing both the threshold-based logic of decision trees and the non-linear representational power of deep learning.

KLEAR is validated through a comprehensive multi-site study involving 2,013 kidney transplant recipients, demonstrating that high-resolution molecular matching significantly outstrips the performance of current standard-of-care matching techniques. We further confirm the clinical utility of KLEAR

through a prospective validation cohort, showcasing its potential to revolutionize donor-recipient matching and drug development through clinical trial enrichment.

2 Related work

Machine learning applications in transplantation have focused on survival analysis using Cox proportional hazards models and on organ discard or delayed graft function prediction (Schliephacke et al., 2026). Schliephacke et al. (2026) demonstrated that consistent data preprocessing and Bayesian hyperparameter optimization can make ensemble models highly effective for predicting kidney discard risk. However, these models often exclude recipient characteristics to facilitate early organ offer evaluation, thereby missing the critical immune interaction between donor and recipient.

Machine learning for tabular data remains challenging, as architectures such as Transformers and CNNs often struggle with the heterogeneous, non-spatial features of medical records. Numerical feature embeddings can allow multi-layer perceptrons and Transformers to compete with gradient-boosted decision trees on tabular benchmarks, and the mapping of scalar values to high-dimensional embeddings is an important design choice (Gorishniy et al., 2023). KLEAR extends this concept by using XGBoost leaf indices as embeddings that preserve the nonlinear interactions learned by the boosting process. Clinical datasets are also characterized by severe class imbalance, where outcomes such as rejection or mortality are rare (Fujiwara et al., 2020). Traditional oversampling methods such as SMOTE can overfit in high-dimensional spaces (Chuang et al., 2026), while generative models provide an alternative. The Majority-Guided VAE proposed by Ai et al. uses majority-class priors to guide minority-sample generation and mitigate model collapse (Ai et al., 2023). KLEAR adopts a similar approach by combining a VAE with GMM density modeling to capture the multimodal distribution of rejection phenotypes. Molecular-level HLA matching provides greater granularity than antigen-level matching (Chou-Wu et al., 2025). HLAMatchmaker and PIRCHE-II measure eplet load and indirect T-cell recognition, respectively, although the relative immunogenicity of these molecular mismatches remains under investigation (Bezstarosti & Heidt, 2025a). KLEAR evaluates the predictive value of these molecular features within a hybrid machine learning pipeline.

3 Clinical data and histocompatibility feature engineering

The KLEAR framework is built upon a multi-center study involving 2,013 adult kidney transplant recipients across three Mayo Clinic sites: Arizona ($n = 971$), Rochester ($n = 443$), and Florida ($n = 599$). Patients with at least one year of follow-up and one recorded biopsy were included to ensure ground-truth outcomes for TCMR and ABMR based on Banff classification scores (Appendix D).

3.1 Cohort characteristics

The high-resolution, imputed-HLA, and low-resolution-HLA cohorts contained 401, 1,263, and 1,340 recipients, with TCMR rates of 6.5%, 13.4%, and 13.4% and ABMR rates of 3.7%, 4.8%, and 4.6%, respectively. Their transplant years, HLA mismatch burden, cPRA, and KDPI distributions are summarized in Table 5 in Appendix B.

3.2 E3 molecular feature (MoF) derivation

To transcend standard allele-level counts, we utilized the E3 computational framework to derive 95 molecular HLA mismatch features from high-resolution (4-digit) HLA typing (Appendix E.2). E3 quantifies the physiochemical and structural differences between donor and recipient HLA molecules at nine loci: HLA-A, -B, -C, -DRB1, -DRB345, -DQA1, -DQB1, -DPA1, and -DPB1.

The E3-MoFs encompass several distinct categories of immunogenicity, including amino acid mismatch load (AML), which measures the raw count of amino acid differences; electrostatic mismatch load (EML), which quantifies differences in the surface charge of HLA molecules; hydrophobicity mismatch load (HML), which assesses residue-level hydrophobicity variation; HLAMatchmaker (EpiL), which measures the total load of mismatched eplets, defined as solvent-accessible amino acid clusters recognized by antibodies; and the PIRCHE-II score, which estimates indirect presentation of donor HLA-derived peptides by recipient HLA Class II molecules to $CD4^+$ T cells.

Crucially, KLEAR derives rejection-specific feature sets. For TCMR, the features include AML, EML, and HML restricted to the α_1 and α_2 domains, the regions of HLA molecules most critical for T-cell receptor recognition. For ABMR, the full-molecule features and humoral metrics, including EpiL and PIRCHE, are utilized to capture B-cell mediated alloimmunity.

4 METHODOLOGY

4.1 PROBLEM FORMULATION

Our objective is to predict transplantation rejection using predictive modeling on a dataset composed of clinical and molecular data. Given a feature vector x representing the features of a donor-recipient pair, we aim to learn a function that performs binary classification and outputs the probability of rejection within the first year after transplantation. Two distinct rejection phenotypes, T cell-mediated rejection (TCMR) and antibody-mediated rejection (ABMR), were studied.

Our pipeline consists of two stages. First, we construct molecular E3 features from donor-recipient HLA mismatch, which capture physicochemical and immunogenic properties of the mismatch and then perform principal component analysis (PCA) to reduce the dimensionality to five principal components (PCs) for TCMR-specific and 12 PCs for ABMR-specific E3 features. Second, we use clinical data combined with the derived E3 PCs as input to a predictive modeling pipeline.

4.2 DATA PREPROCESSING

The input data consists of categorical features with varying cardinalities and numerical features. To ensure efficient model training and prevent data leakage, all preprocessing steps are performed independently within each training fold.

Numerical features. The median value from the training fold was used to replace any missing numerical values. Using standard scalar transformation, features are standardized to a mean of zero and unit variance.

Categorical features. The most frequent category within the training fold was used to replace any missing categorical values. To account for differences in cardinalities, we use two different encoders. High-cardinality features are encoded using target encoding. Low-cardinality features are encoded using one-hot encoding.

4.3 OVERSAMPLING METHOD

Severe class imbalance or a lack of data is the primary bottleneck in all clinical prediction models. To address this, we combine a Variational Autoencoder (VAE) with a Gaussian Mixture Model (GMM) to generate minority-class samples. For a minority-class feature vector x_m, the encoder $q_\phi(z \mid x_m)$ learns a latent representation and the decoder $p_\theta(x_m \mid z)$ reconstructs the input. The VAE objective is

$$\mathcal{L}_{\text{VAE}} = \mathbb{E}_{q_\phi(z|x_m)} \left[\|x_m - p_\theta(z)\|_2^2 \right] + D_{\text{KL}} \left(q_\phi(z \mid x_m) \,\|\, p(z) \right), \tag{1}$$

where $p(z)$ is a standard normal prior. Latent samples drawn from this prior are decoded and combined with the observed minority examples to form an enhanced minority set.

Because direct prior sampling may not capture a multimodal minority distribution, we fit a GMM to the enhanced set:

$$p(x) = \sum_{k=1}^{K} \pi_k \mathcal{N}(x \mid \mu_k, \Sigma_k), \tag{2}$$

where K is the number of components and π_k, μ_k, and Σ_k are their weights, means, and covariance matrices. Samples from this learned mixture are added to the original training data until the outcome classes are balanced. VAE fitting, GMM fitting, and synthetic sampling are performed independently within each training fold to prevent data leakage.

4.4 XGBOOST LEAF INDICES

Complex nonlinear relationships in the data are represented using XGBoost, whose tree structure can represent feature interactions. We train an XGBoost model on the processed and oversampled data to learn these interactions.

For each input x, the trained XGBoost model assigns it to a leaf node in every tree, producing a vector of leaf indices:

$$\phi(x) = [l_1(x), l_2(x), \ldots, l_T(x)], \tag{3}$$

where $l_t(x)$ denotes the leaf index assigned by the t-th tree and T is the number of trees. These leaf indices effectively represent the nonlinear feature interactions learned.

The leaf indices are categorical variables and encoded using one-hot encoding. The resulting leaf embeddings are concatenated with the original input features to form a combined feature vector:

$$X_{\text{combined}} = [X_{\text{original}}, \phi_{\text{one-hot}}(x)]. \tag{4}$$

The combined feature vector is used as input to a dense neural network for prediction. Leaf embeddings are generated within each training fold after fitting XGBoost on the respective fold's training data. Leaf embeddings are also generated for the validation and test samples using the training data fitted XGBoost model and encoder to prevent data leakage.

4.5 DNN

The primary classification model is a dense neural network trained on the synthetic and original samples. The input vectors consist of the donor-patient data, E3-MoFs, and the XGBoost leaf embeddings.

The neural network is composed of two hidden layers with ReLU activation functions and dropout regularization to combat overfitting. The output layer outputs a logit, which is transformed into a probability using a sigmoid function:

$$\hat{y} = \sigma(s) = \frac{1}{1 + \exp(-s)}. \tag{5}$$

Focal loss is used to combat the heavy class imbalance. Focal loss emphasizes minority samples by weighing the majority samples less. The loss function is defined as:

$$\mathcal{L}_{\text{focal}} = -\alpha(1 - \hat{y})^{\gamma} y \log(\hat{y}) - (1 - y)\hat{y}^{\gamma} \log(1 - \hat{y}), \tag{6}$$

where $y \in \{0, 1\}$ is the ground-truth label, $\hat{y}$ is the predicted probability, and $\alpha \in [0, 1]$ and γ are hyperparameters controlling class weighting and focusing strength.

The complete KLEAR training procedure is provided in Algorithm 1 in Appendix C.

4.6 MODEL TRAINING

The model is optimized using the Adam optimizer with mini-batch gradient descent. To prevent overfitting, early stopping is applied based on validation performance. Training stops when validation loss does not improve for a fixed number of epochs. The model checkpoint with the highest performance is saved. Early stopping is applied across the neural network, VAE and GMM, and XGBoost models. The models were trained using 5-fold cross-validation with Bayesian hyperparameter optimization via the Optuna framework. Subsequently, the models underwent recalibration via isotonic calibration (Appendix F). All experiments are run on an institutional high-performance computing cluster with 128 CPU cores and an NVIDIA RTX A4000 GPU node.

5 EXPERIMENTS

The four machine learning classifiers were trained on the high-resolution dataset. Model performance was evaluated to construct KLEAR and elucidate the importance of high-resolution HLA typing versus low-resolution HLA typing in predicting TCMR and ABMR.

5.1 ALGORITHMIC PERFORMANCE BENCHMARKING

KLEAR's performance was compared against logistic regression, random classifiers, and standalone versions of its constituent algorithms. Because rejection is rare, AUPRC is the primary metric and should be interpreted relative to event prevalence; ROC-AUC and macro F1 are secondary summaries. Future revisions should include confidence intervals and statistical comparisons across folds for all primary baselines. Table 1 summarizes the main benchmarking results.

Models were trained on the high-resolution HLA typing dataset ($n = 319$). The ML classifier with the highest AUPRC for each outcome is bolded.

Table 1: Comparison of ML classifiers for TCMR and ABMR prediction. Models were trained on the high-resolution HLA typing dataset ($n = 319$). The ML classifier with the highest AUPRC for each outcome is bolded.

Target outcome	ML classifier	AUPRC [95% CI]	Macro F1 [95% CI]	ROC-AUC [95% CI]
TCMR ($n = 22/319$)	**XGBoost + DNN**	**0.35 [0.18–0.54]**	**0.59 [0.53–0.66]**	**0.63 [0.48–0.77]**
	XGBoost	0.26 [0.10–0.45]	0.66 [0.53–0.78]	0.43 [0.26–0.60]
	DNN	0.17 [0.07–0.32]	0.28 [0.24–0.32]	0.58 [0.46–0.70]
	Logistic regression	0.26 [0.11–0.45]	0.63 [0.54–0.73]	0.55 [0.40–0.71]
	Elastic net logistic regression	0.13 [0.07–0.28]	0.42 [0.38–0.47]	0.61 [0.48–0.74]
	Random classifier	0.07	0.39	0.50
ABMR ($n = 12/319$)	**XGBoost + DNN**	**0.30 [0.06–0.54]**	**0.57 [0.50–0.65]**	**0.65 [0.46–0.81]**
	XGBoost	0.11 [0.04–0.27]	0.59 [0.51–0.69]	0.57 [0.38–0.76]
	DNN	0.26 [0.07–0.53]	0.61 [0.52–0.69]	0.68 [0.51–0.83]
	Logistic regression	0.11 [0.04–0.27]	0.33 [0.29–0.36]	0.63 [0.48–0.78]
	Elastic net logistic regression	0.12 [0.04–0.35]	0.49 [0.48–0.49]	0.61 [0.38–0.83]
	Random classifier	0.04	0.36	0.50

5.2 RESOLUTION-DEPENDENT PERFORMANCE GAIN

A key hypothesis of this study is that high-resolution HLA typing provides superior predictive information compared to standard clinical typing. To test this, we reconstructed low-resolution and imputed-high-resolution datasets for a fixed cohort of 285 patients. Table 2 summarizes the direct comparisons.

Table 2: Performance comparisons of XGBoost + DNN across different sets of input variables for TCMR and ABMR prediction. For all datasets, XGBoost + DNN was trained on the same patient cohort ($n = 285$) for direct comparisons. CIs = confidence intervals; DRCs = donor–recipient characteristics; MoFs = molecular features.

Target outcome	Input variables	AUPRC [95% CI]	Macro F1 [95% CI]	ROC-AUC [95% CI]
TCMR ($n = 21/285$) XGBoost + DNN	**DRCs + full E3-TCMR-MoFs**	**0.264 [0.105–0.449]**	**0.63 [0.51–0.73]**	**0.46 [0.30–0.62]**
	Full E3-TCMR-MoFs	0.213 [0.108–0.356]	0.59 [0.52–0.66]	0.67 [0.53–0.80]
	Partial E3-TCMR-MoFs	0.194 [0.089–0.360]	0.62 [0.54–0.71]	0.57 [0.42–0.73]
	DRCs + partial E3-TCMR-MoFs	0.190 [0.085–0.351]	0.62 [0.51–0.72]	0.55 [0.40–0.68]
	DRCs	0.149 [0.070–0.290]	0.59 [0.48–0.69]	0.51 [0.38–0.66]
	HLAMatchMaker score	0.114 [0.068–0.193]	0.43 [0.39–0.48]	0.53 [0.39–0.66]
	PIRCHE-II score	0.095 [0.067–0.139]	0.48 [0.43–0.53]	0.54 [0.41–0.67]
	HLA mismatch count	0.092 [0.066–0.141]	0.42 [0.38–0.47]	0.54 [0.42–0.67]
ABMR ($n = 12/285$) XGBoost + DNN	**DRCs + full E3-ABMR-MoFs**	**0.263 [0.049–0.505]**	**0.59 [0.50–0.67]**	**0.56 [0.35–0.76]**
	Full E3-ABMR-MoFs	0.238 [0.043–0.461]	0.62 [0.52–0.74]	0.54 [0.35–0.73]
	Partial E3-ABMR-MoFs	0.172 [0.065–0.349]	0.58 [0.51–0.66]	0.67 [0.51–0.83]
	DRCs	0.170 [0.038–0.394]	0.55 [0.47–0.64]	0.53 [0.35–0.71]
	DRCs + partial E3-ABMR-MoFs	0.165 [0.055–0.363]	0.64 [0.52–0.76]	0.62 [0.45–0.80]
	PIRCHE-II score	0.091 [0.049–0.160]	0.55 [0.49–0.63]	0.64 [0.48–0.81]
	HLAMatchMaker score	0.074 [0.039–0.133]	0.51 [0.46–0.57]	0.55 [0.36–0.73]
	HLA mismatch count	0.069 [0.043–0.120]	0.27 [0.24–0.31]	0.60 [0.47–0.73]

For all datasets, XGBoost + DNN was trained on the same patient cohort ($n = 285$) for direct comparisons. DRCs = donor-recipient characteristics; MoFs = molecular features.

5.3 SITE-SPECIFIC PERFORMANCE ANALYSIS

KLEAR's performance varied between Mayo Clinic sites, with mean AUPRC values consistently higher at Mayo Clinic Florida than at Mayo Clinic Arizona for both TCMR and ABMR (Table 3).

This difference may be attributed, in part, to the slightly higher prevalence of positive cases at Mayo Clinic Florida for model training thereby improving model robustness.

Table 3: Comparison of KLEAR across Mayo Clinic sites for TCMR and ABMR prediction. Performance of KLEAR was assessed separately for Mayo Clinic Florida (n=106) and Mayo Clinic Arizona (n=213) using the high-resolution HLA typing dataset (n=319).

Target outcome	Center	AUPRC		Macro F1		ROC-AUC	
		Random classifier	KLEAR [95% CI]	Random classifier	KLEAR [95% CI]	Random classifier	KLEAR [95% CI]
TCMR	Florida ($n = 13/106$)	0.12	0.45 [0.23–0.70]	0.42	0.71 [0.54–0.83]	0.50	0.66 [0.46–0.84]
	Arizona ($n = 9/213$)	0.04	0.18 [0.04–0.50]	0.37	0.58 [0.49–0.74]	0.50	0.56 [0.34–0.79]
ABMR	Florida ($n = 3/106$)	0.03	0.37 [0.04–1.00]	0.36	0.75 [0.49–1.00]	0.50	0.68 [0.40–1.00]
	Arizona ($n = 9/213$)	0.04	0.26 [0.06–0.57]	0.37	0.62 [0.48–0.77]	0.50	0.64 [0.41–0.86]

6 Interpretability and variable importance analysis

To ensure that KLEAR provides clinically plausible insights, we conducted SHapley Additive exPlanations (SHAP) analysis (Appendix G).

6.1 Top predictors for TCMR

For cellular rejection, the model relied on a mixture of racial factors, clinical status, and molecular mismatches:

1. The recipient/donor race is a significant contributor, likely reflecting underlying immunogenetic diversity and systemic disparities.
2. The TCMR-E3-MoF PC3 was primarily driven by the hydrophobicity and electrostatic load at the HLA-B locus.
3. The allele-level HLA MMs are raw mismatch counts that remained a robust baseline signal.
4. The recipient CMV serostatus is a known modulator of T-cell activation and inflammation.

6.2 Top predictors for ABMR

For antibody-mediated rejection, the model was dominated by humoral risk factors:

1. The HLA allele MMs show high sensitivity to mismatches at the DQ locus, which are notoriously immunogenic.
2. The ABMR-E3-MoF PC3 and PC6 are driven by Epitope Load (EpiL) for HLA Class I and HLA-DPB1.
3. The recipient cPRA and BMI reflect higher sensitization levels and metabolic status, which were strong predictors of humoral risk.

These findings underscore the necessity of moving beyond simple antigen counts to capture the influence of histocompatibility mismatches at the molecular and eplet levels.

7 Prospective clinical validation and clinical utility

Between September 2022 and December 2023, we conducted a prospective validation study at Mayo Clinic Florida involving 82 patients (Appendix H). This cohort was monitored for at least one year post-transplant for rejection events.

7.1 Prospective model performance

The TCMR and ABMR models maintained superior performance over random classifiers, with AUPRC values reported in Table 4. While these absolute values appear low due to the low incidence

Table 4: Prospective validation of KLEAR. The table shows the mean ± standard deviation of AUPRC over 1,000 bootstraps for KLEAR compared to random classifiers in parentheses, the numbers of true positive (TP), negative (TN), false positive (FP), and negative (FN).

Outcome	AUPRC	Specificity	Sensitivity	TN	FP	FN	TP
TCMR	0.075 ± 0.021 (0.049)	59.0%	75.0%	46	32	1	3
ABMR	0.077 ± 0.024 (0.037)	39.2%	100%	31	48	0	3

of rejection, they represent 1.5-fold and 2.0-fold improvements over random guessing in a highly imbalanced, real-world setting (Table 4 and Figure 2).

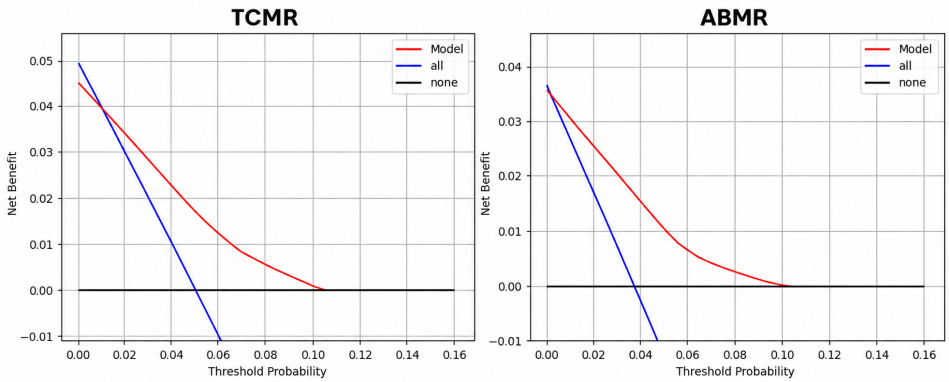

Figure 2: Decision curve analysis. Decision curves present the net benefit of using KLEAR for predicting TCMR and ABMR compared to treating all or no patients.

7.2 Clinical utility and decision curve analysis

To evaluate the practical benefit of KLEAR, we performed Decision Curve Analysis (DCA). DCA assesses the "net benefit" of using a predictive model to guide clinical intervention across a range of risk thresholds. KLEAR demonstrated a positive net benefit for TCMR across thresholds of 0.01–0.10 and for ABMR across thresholds of 0.005–0.10. This indicates that using KLEAR to identify high-risk patients for intensive monitoring or biopsy is clinically superior to a "treat-all" or "treat-none" strategy.

8 Broader impact and ethical considerations

The deployment of AI in transplantation requires careful ethical scrutiny (Kourounis et al., 2026). KLEAR's inclusion of recipient and donor race as top predictors highlights the potential for algorithmic bias if not handled transparently (Kourounis et al., 2026). We have taken concrete steps to mitigate this by using a diverse multi-site training set and oversampling techniques to ensure adequate representation of minority phenotypes.

Furthermore, the "responsible AI" framework employed in KLEAR prioritizes transparency. By providing SHAP-based interpretations, we empower clinicians to understand why a particular patient is at high risk, rather than presenting a "black box" prediction. This is critical for maintaining patient-physician trust and ensuring that AI serves as a tool for decision support rather than a replacement for human judgment (Lozano-Suarez et al., 2025).

Limitations include the retrospective design, a small prospective validation cohort (n=82), and potential selection bias due to the requirement of at least one biopsy. Prospective multicenter validation is needed to confirm generalizability and assess cost-effectiveness. Future iterations of KLEAR could move beyond pre-transplant prediction to simulate how different post-transplant interventions might alter the risk trajectory for an individual patient (Vivek & Papalois, 2025). Integrating KLEAR with

longitudinal electronic health records (EHRs) via federated learning architectures could further refine its accuracy while preserving patient privacy.

9 CONCLUSION

KLEAR is a comprehensive AI-based predictive suite that integrates recipient and donor characteristics with rejection-type-specific E3-MoFs to assess the risk of TCMR and ABMR during the first year following deceased-donor kidney transplantation. As a promising preliminary model, KLEAR creates a pathway toward future prospective validation at a larger scale in independent external cohorts to enable eventual clinical implementation for personalized pre-transplant risk stratification that could inform immunosuppression, surveillance, and organ allocation strategies. KLEAR has the potential to (1) improve donor–recipient matching by reducing acute rejection risk, (2) inform clinical decision-making and patient management by identifying high-risk patients who may benefit from more intensive post-transplant monitoring, and (3) facilitate drug development through clinical trial enrichment. KLEAR is designed to refine, not replace, existing risk stratification, with particular utility for intermediate-risk patients, supporting more targeted monitoring and reducing unnecessary interventions.

AI USE STATEMENT

Generative AI tools were used only to polish the paper's writing and to generate the diagram in Figure 1. They were not used to formulate the research question or hypotheses, design the study or methodology, generate or clean the study data, implement the models, conduct the statistical analyses, or interpret the results. The authors reviewed and revised all AI-assisted text and verified that Figure 1 accurately represents the implemented pipeline. The authors take full responsibility for the paper's content, claims, and AI-assisted artifact.

ETHICS STATEMENT

This study analyzes clinical and molecular information from kidney transplant recipients, making patient privacy, appropriate governance of human-subject data, and equitable model performance central ethical considerations. Results are reported in aggregate, and the publicly described artifact is the anonymized training and evaluation pipeline rather than patient-level clinical data. Donor and recipient race contribute to the model and may encode immunogenetic structure, unequal access to care, or other unmeasured social factors; these associations should not be interpreted causally and require subgroup evaluation before clinical use. The retrospective design, biopsy-based selection, small prospective cohort, and very small numbers of prospective rejection events limit the evidence for generalizability and equitable performance. KLEAR is therefore presented as a research-stage decision-support approach that must not independently determine organ acceptance, immunosuppression, surveillance, or biopsy decisions. Larger independent multicenter studies, fairness analyses, calibration assessment, and evaluation with clinicians and patients are required before deployment.

REPRODUCIBILITY STATEMENT

We support reproducibility through an anonymized implementation of the KLEAR training and evaluation pipeline provided in Appendix A. The main text specifies the cohort construction and molecular features, fold-wise imputation and encoding, VAE–GMM oversampling, XGBoost leaf embeddings, dense neural network, focal-loss objective, five-fold cross-validation, Bayesian hyperparameter optimization, early stopping, and isotonic calibration. Appendix C summarizes the complete training procedure; Appendices B, D, and E document the cohorts, study design, and molecular features; and Appendices F, G, and H provide supporting calibration, interpretability, and prospective-validation results. Preprocessing, oversampling, feature construction, and model fitting are performed within each training fold to reduce data leakage.

REFERENCES

Qingzhong Ai, Pengyun Wang, Lirong He, Liangjian Wen, Lujia Pan, and Zenglin Xu. Generative oversampling for imbalanced data via majority-guided vae, 2023. URL https://arxiv.org/abs/2302.10910.

Suzanne Bezstarosti and Sebastiaan Heidt. The Progress and Challenges of Implementing HLA Molecular Matching in Clinical Practice. *Transplant international : official journal of the European Society for Organ Transplantation*, 38:14716, 2025a. ISSN 1432-2277. doi: 10.3389/ti.2025.14716.

Suzanne Bezstarosti and Sebastiaan Heidt. The Progress and Challenges of Implementing HLA Molecular Matching in Clinical Practice. *Transplant international : official journal of the European Society for Organ Transplantation*, 38:14716, 2025b. ISSN 1432-2277. doi: 10.3389/ti.2025.14716.

Elaine Chou-Wu, Matthias Niemann, Danny Youngs, and Idoia Gimferrer. De novo donor-specific anti-hla antibody risk stratification in kidney transplantation using a combination of b cell and t cell molecular mismatch assessment. *Frontiers in Immunology*, Volume 16 - 2025, 2025. ISSN 1664-3224. doi: 10.3389/fimmu.2025.1508796. URL https://www.frontiersin.org/journals/immunology/articles/10.3389/fimmu.2025.1508796.

Chien-Wei Chuang, Chung-Kuan Wu, Chao-Hsin Wu, Ben-Chang Shia, and Mingchih Chen. Enhancing model generalizability in medical artificial intelligence: Systematic comparison of categorical encoding and sampling techniques for imbalanced data. *JMIR Med Inform*, 14:e75655, April 2026.

Zeynep Demir, Marc Raynaud, Gillian Divard, Kevin Louis, Agathe Truchot, Matthias Niemann, Renata Ponsirenas, Olivier Aubert, Arnaud Del Bello, Alexandre Hertig, Dany Anglicheau, Bethany Dale, Nassim Kamar, Massimo Mangiola, Adriana Zeevi, Carmen Lefaucheur, and Alexandre Loupy. Impact of HLA evolutionary divergence and donor-recipient molecular mismatches on antibody-mediated rejection of kidney allografts. *Nature Communications*, 16(1):5692, jul 2025. ISSN 2041-1723. doi: 10.1038/s41467-025-60485-y.

Koichi Fujiwara, Yukun Huang, Kentaro Hori, Kenichi Nishioji, Masao Kobayashi, Mai Kamaguchi, and Manabu Kano. Over- and under-sampling approach for extremely imbalanced and small minority data problem in health record analysis. *Frontiers in Public Health*, Volume 8 - 2020, 2020. ISSN 2296-2565. doi: 10.3389/fpubh.2020.00178. URL https://www.frontiersin.org/journals/public-health/articles/10.3389/fpubh.2020.00178.

Manuel Moreno Gonzales, Andrew Bentall, Walter K Kremers, Mark D Stegall, and Richard Borrows. Predicting Individual Renal Allograft Outcomes Using Risk Models with 1-Year Surveillance Biopsy and Alloantibody Data. *Journal of the American Society of Nephrology : JASN*, 27(10): 3165–3174, oct 2016. ISSN 1533-3450. doi: 10.1681/ASN.2015070811.

Yury Gorishniy, Ivan Rubachev, and Artem Babenko. On embeddings for numerical features in tabular deep learning, 2023. URL https://arxiv.org/abs/2203.05556.

Sundaram Hariharan, Ajay K Israni, and Gabriel Danovitch. Long-Term Survival after Kidney Transplantation. Reply. *The New England journal of medicine*, 386(5):499–500, feb 2022. ISSN 1533-4406. doi: 10.1056/NEJMc2115207.

Xiang He, Jason Moore, Shazia Shabir, Mark A Little, Paul Cockwell, Simon Ball, Xiang Liu, Atholl Johnston, and Richard Borrows. Comparison of the predictive performance of eGFR formulae for mortality and graft failure in renal transplant recipients. *Transplantation*, 87(3):384–92, feb 2009. ISSN 1534-6080. doi: 10.1097/TP.0b013e31819004a1.

Stanley C. Jordan, Jua Choi, and Ashley Vo. Kidney transplantation in highly sensitized patients. *British Medical Bulletin*, 114(1):113–125, jun 2015. ISSN 0007-1420. doi: 10.1093/bmb/ldv013.

Vadim Jucaud, Abraham Shaked, Michele DesMarais, Peter Sayre, Sandy Feng, Josh Levitsky, and Matthew J. Everly. Prevalence and Impact of De Novo Donor-Specific Antibodies During a Multicenter Immunosuppression Withdrawal Trial in Adult Liver Transplant Recipients. *Hepatology*, 69 (3):1273–1286, mar 2019. ISSN 0270-9139. doi: 10.1002/hep.30281.

Vadim Jucaud, Lorita M. Rebellato, Kimberly P. Briley, Carl E. Haisch, Scott A. Kendrick, Heather Jones, Kristel Mclawhorn, David Leeser, and Matthew J. Everly. DO WE PREDICT MISMATCHES THAT INDUCE DE NOVO DSA OR DO WE PREDICT THE ONES THAT DO NOT? *Transplantation*, 104(S3):S49–S50, sep 2020. ISSN 0041-1337. doi: 10.1097/01.tp.0000698508.30965.3e.

Bruce Kaplan, Jesse Schold, and Herwig-Ulf Meier-Kriesche. Poor predictive value of serum creatinine for renal allograft loss. *American journal of transplantation : official journal of the American Society of Transplantation and the American Society of Transplant Surgeons*, 3(12): 1560–5, dec 2003. ISSN 1600-6135. doi: 10.1046/j.1600-6135.2003.00275.x.

Amanda Klein, Alexandre Loupy, Mark Stegall, Ilkka Helanterä, Luke Kosinski, Eric Frey, Olivier Aubert, Gillian Divard, Kenneth Newell, Herwig-Ulf Meier-Kriesche, Roslyn B. Mannon, Thomas Dumortier, Varun Aggarwal, Jagdeep T. Podichetty, Inish O'Doherty, Ahmed Osama Gaber, and William E. Fitzsimmons. Qualifying a novel clinical trial endpoint (iBOX) predictive of long-term kidney transplant outcomes. *American Journal of Transplantation*, 23(10):1496–1506, oct 2023. ISSN 16006135. doi: 10.1016/j.ajt.2023.04.018.

Georgios Kourounis, Stephen Gilbert, Simon R. Knight, Amanda Leal, Jackie Leach Scully, Alexandre Loupy, Dominique E. Martin, Evgenia Preka, Nadia Primc, Fernando Seoane Martinez, Helena Webb, Gabriel C. Oniscu, and Colin Wilson. Shaping the future of ai in organ transplantation: Position paper of the european society for organ transplantation. *Transplant International*, Volume 39 - 2026, 2026. ISSN 1432-2277. doi: 10.3389/ti.2026.16316. URL https://www.frontierspartnerships.org/journals/transplant-international/articles/10.3389/ti.2026.16316.

Alexandre Loupy, Olivier Aubert, Babak J Orandi, Maarten Naesens, Yassine Bouatou, Marc Raynaud, Gillian Divard, Annette M Jackson, Denis Viglietti, Magali Giral, Nassim Kamar, Olivier Thaunat, Emmanuel Morelon, Michel Delahousse, Dirk Kuypers, Alexandre Hertig, Eric Rondeau, Elodie Bailly, Farsad Eskandary, Georg Böhmig, Gaurav Gupta, Denis Glotz, Christophe Legendre, Robert A Montgomery, Mark D Stegall, Jean-Philippe Empana, Xavier Jouven, Dorry L Segev, and Carmen Lefaucheur. Prediction system for risk of allograft loss in patients receiving kidney transplants: international derivation and validation study. *BMJ (Clinical research ed.)*, 366:l4923, sep 2019a. ISSN 1756-1833. doi: 10.1136/bmj.l4923.

Alexandre Loupy, Olivier Aubert, Babak J. Orandi, Maarten Naesens, Yassine Bouatou, Marc Raynaud, Gillian Divard, Annette M. Jackson, Denis Viglietti, Magali Giral, Nassim Kamar, Olivier Thaunat, Emmanuel Morelon, Michel Delahousse, Dirk Kuypers, Alexandre Hertig, Eric Rondeau, Elodie Bailly, Farsad Eskandary, Georg Böhmig, Gaurav Gupta, Denis Glotz, Christophe Legendre, Robert A. Montgomery, Mark D. Stegall, Jean Philippe Empana, Xavier Jouven, Dorry L. Segev, and Carmen Lefaucheur. Prediction system for risk of allograft loss in patients receiving kidney transplants: International derivation and validation study. *The BMJ*, 366:1–12, 2019b. ISSN 17561833. doi: 10.1136/bmj.l4923.

Nicolás Lozano-Suarez, Julia Andrea Gomez-Montero, Maritza Jiménez-Gómez, Santiago Cabas, Nicolás Giron-Londoño, Andrea García-López, and Fernando Giron-Luque. Bioethical challenges in the integration of artificial intelligence in transplant surgery 4.0: A scoping review. *Digit Health*, 11:20552076251351700, June 2025.

Madhav C Menon, Barbara Murphy, and Peter S Heeger. Moving Biomarkers toward Clinical Implementation in Kidney Transplantation. *Journal of the American Society of Nephrology : JASN*, 28(3):735–747, mar 2017. ISSN 1533-3450. doi: 10.1681/ASN.2016080858.

Muhammed Mubarak, Amber Raza, Rahma Rashid, and Shaheera Shakeel. Evolution of human kidney allograft pathology diagnostics through 30 years of the Banff classification process. *World journal of transplantation*, 13(5):221–238, sep 2023. ISSN 2220-3230. doi: 10.5500/wjt.v13.i5.221.

OPTN. Organ transplants OPTN, 2023. URL https://www.hrsa.gov/optn?from=optn.transplant.hrsa.gov.

C. Puttarajappa, J. Ujhazy, H. Morford, V. Kumar, M. Greenwood, L. Gragert, M. Bettinotti, Y. Kyeso, O. Moussa, L. Bow, M. Mankowski, T. Yamada, Q. Xu, M. Klem, and V. Dharnidharka. HLA Molecular Mismatch and Risk of Adverse Kidney Transplant Outcomes - A Systematic Review. *American Journal of Transplantation*, 25(8):S542, aug 2025. ISSN 16006135. doi: 10.1016/j.ajt.2025.07.1258.

Eva Santos, Katrina Spensley, Nicola Gunby, Judith Worthington, Candice Roufosse, Arthi Anand, and Michelle Willicombe. Application of HLA molecular level mismatching in ethnically diverse kidney transplant recipients receiving a steroid-sparing immunosuppression protocol. *American Journal of Transplantation*, 24(7):1218–1232, jul 2024. ISSN 16006135. doi: 10.1016/j.ajt.2024.02.019.

Peer Schliephacke, Hannah Schult, Leon Mizera, Judith Würfel, Gunter Grieser, Axel Rahmel, Carl-Ludwig Fischer-Fröhlich, and Antje Jahn-Eimermacher. Comparative evaluation of machine learning models for predicting donor kidney discard, 2026. URL https://arxiv.org/abs/2602.21876.

M D Stegall, R E Morris, R R Alloway, and R B Mannon. Developing New Immunosuppression for the Next Generation of Transplant Recipients: The Path Forward. *American journal of transplantation : official journal of the American Society of Transplantation and the American Society of Transplant Surgeons*, 16(4):1094–101, apr 2016. ISSN 1600-6143. doi: 10.1111/ajt.13582.

Flavio Vincenti, Lionel Rostaing, Joseph Grinyo, Kim Rice, Steven Steinberg, Luis Gaite, Marie-Christine Moal, Guillermo A Mondragon-Ramirez, Jatin Kothari, Martin S Polinsky, Herwig-Ulf Meier-Kriesche, Stephane Munier, and Christian P Larsen. Belatacept and Long-Term Outcomes in Kidney Transplantation. *The New England journal of medicine*, 374(4):333–43, jan 2016. ISSN 1533-4406. doi: 10.1056/NEJMoa1506027.

Kavyesh Vivek and Vassilios Papalois. Ai and machine learning in transplantation. *Transplantology*, 6(3), 2025. ISSN 2673-3943. doi: 10.3390/transplantology6030023. URL https://www.mdpi.com/2673-3943/6/3/23.

WHO. The global database on donation and transplantation, 2025. URL https://www.transplant-observatory.org/.

APPENDIX

- Appendix A: Code availability . . . . . p. 14
- Appendix B: Cohort characteristics . . . . . p. 14
- Appendix C: KLEAR training algorithm . . . . . p. 14
- Appendix D: Study design . . . . . p. 15
- Appendix E: Development cohort with high-resolution HLA typing . . . . . p. 17
- Appendix F: Model calibration . . . . . p. 22
- Appendix G: SHAP analysis for input feature importance . . . . . p. 23
- Appendix H: Prospective validation cohort . . . . . p. 24

A CODE AVAILABILITY

An anonymized version of the KLEAR training and evaluation pipeline is available at:

`https://anonymous.4open.science/r/klear-1`

B COHORT CHARACTERISTICS

Table 5: Clinical characteristics of the study cohorts.

Characteristic	High-res HLA	Imputed HLA	Low-res HLA
Transplant years	2020–2023	2020–2022	2020–2022
Cohort size	401	1263	1340
TCMR, n (%)	26 (6.5)	169 (13.4)	179 (13.4)
ABMR, n (%)	15 (3.7)	61 (4.8)	61 (4.6)
HLA mismatch, median [IQR]	12 [10, 14]	8 [7, 10]	8 [7, 10]
cPRA, median [IQR]	0.07 [0.00, 41.10]	0.00 [0.00, 37.17]	0.00 [0.00, 41.15]
KDPI, median [IQR]	43 [24, 63]	43 [22, 64]	43 [22, 63.25]

C KLEAR TRAINING ALGORITHM

Algorithm 1 summarizes the complete fold-wise training, optimization, and calibration procedure.

Algorithm 1 KLEAR training pipeline

Input: Dataset $\mathcal{D} = \{(H_i, c_i, y_i)\}_{i=1}^{N}$
Compute E3 mismatch features: $m_i \leftarrow \mathrm{E3}(H_i)$
Apply PCA to E3 features
Construct feature vectors: $x_i \leftarrow [c_i, \mathrm{PCA}(m_i)]$
for each cross-validation fold **do**
    Preprocess training and validation data
    Extract minority samples: $X_m \leftarrow \{x_i : y_i = 1\}$
    Train VAE on X_m
    Sample latent vectors: $z \sim \mathcal{N}(0, I)$
    Generate VAE samples: $\hat{X}_m \leftarrow p_\theta(x_m|z)$
    Form enhanced minority set: $X_{\mathrm{enhanced}} \leftarrow [X_m, \hat{X}_m]$
    Fit GMM on X_{enhanced}
    Sample synthetic minority data: $X^* \sim p(x)$
    Form oversampled dataset: $\mathcal{D}_{\mathrm{res}} \leftarrow \mathcal{D}_{\mathrm{train}} \cup X^*$
    Train XGBoost on $\mathcal{D}_{\mathrm{res}}$
    Extract leaf indices: $\phi(x) = [\ell_1(x), \ldots, \ell_T(x)]$
    One-hot encode leaf embeddings
    Construct combined features: $x_{\mathrm{combined}} \leftarrow [x, \phi_{\mathrm{onehot}}(x)]$
    Train DNN using focal loss
    Apply early stopping and evaluate on validation fold
end for
Select best hyperparameters using Optuna
Apply isotonic calibration
Output: Final calibrated prediction model

D STUDY DESIGN

D.1 PATIENT SELECTION FLOWCHART

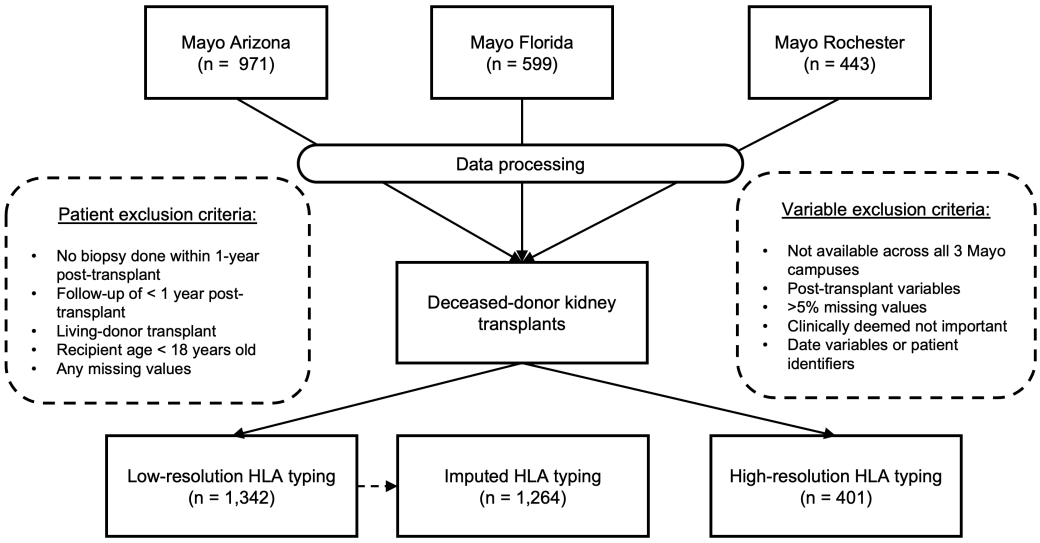

Figure 3: Patient selection flowchart. Recipient and donor data were collected from the three Mayo Clinic campuses: Mayo Arizona, Mayo Florida, and Mayo Rochester. The collected data were processed and harmonized before merging, based on the patient and variable exclusion criteria shown above. The data were then categorized by HLA typing resolution into three distinct groups: low-resolution, imputed, and high-resolution HLA typing datasets.

D.2 MODEL DEVELOPMENT STRATEGY

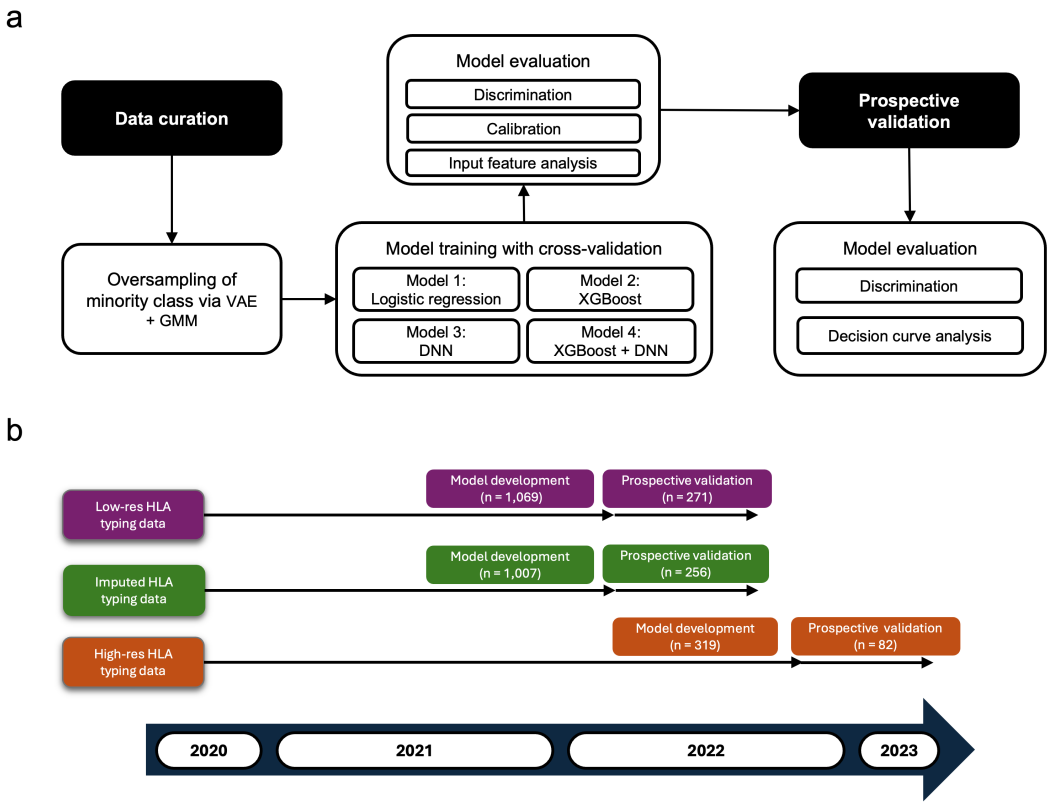

Figure 4: Model development strategy. a, Diagram outlining the overall modeling strategy. The curated dataset underwent class balancing through oversampling of minority cases followed by model training and performance evaluation and model selection. The best-performing models were then evaluated using a prospective validation cohort. b, Timeline illustrating the dataset construction across three HLA typing categories: low-resolution, imputed, and high-resolution. For each dataset, cases occurring prior to the transplant date cutoff were used for model development. Prospective observational studies conducted after the cutoff were then used to validate the predictions of the model.

E DEVELOPMENT COHORT WITH HIGH-RESOLUTION HLA TYPING

E.1 PATIENT DEMOGRAPHICS

Table 6: Demographic and clinical characteristics of the patient cohort with high-resolution HLA typing.

Characteristic	Development cohort ($n = 319$)
Recipient characteristics	
Male, n (%)	186 (58.3)
Age, median [IQR]	57.00 [44.00, 65.00]
Non-Hispanic/Latino, n (%)	252 (79.0)
Race: Amer Ind/Alaska Native, n (%)	9 (2.8)
Race: Asian, n (%)	24 (7.5)
Race: Black, n (%)	86 (27.0)
Race: Hispanic, n (%)	57 (17.9)
Race: Multiracial/Native Hawaiian/Other Pacific Islander, n (%)	5 (1.6)
Race: White, n (%)	137 (42.9)
Race: Unknown/choose not to disclose, n (%)	1 (0.3)
Pre-transplant diabetes, n (%)	120 (37.6)
Previous kidney transplant, n (%)	43 (13.5)
Pretransplant dialysis, n (%)	258 (80.9)
BMI at transplant, median [IQR]	27.24 [24.42, 31.95]
cPRA, median [IQR]	0.26 [0.00, 46.95]
Days on waitlist, median [IQR]	1011.00 [403.00, 1890.50]
CMV, n (%)	230 (72.1)
EBV, n (%)	316 (99.1)
CMV mismatch, n (%)	124 (38.9)
EBV mismatch, n (%)	136 (42.6)
Blood type A, n (%)	107 (33.5)
Blood type AB, n (%)	16 (5.0)
Blood type B, n (%)	69 (21.6)
Blood type O, n (%)	127 (39.8)
HLA mismatch, median [IQR]	12.00 [10.00, 14.00]
Induction therapy: Thymoglobulin, n (%)	73 (22.9)
Induction therapy: Simulect, n (%)	93 (29.2)
Induction therapy: Campath, n (%)	153 (48.0)
1-year TCMR, n (%)	22 (6.9)
1-year ABMR, n (%)	12 (3.8)
Donor characteristics	
Age, median [IQR]	41.00 [31.00, 51.00]
Non-Hispanic/Latino, n (%)	251 (78.7)
Race: Amer Ind/Alaska Native, n (%)	7 (2.2)
Race: Asian, n (%)	7 (2.2)
Race: Black, n (%)	24 (7.5)
Race: Hispanic, n (%)	57 (17.9)
Race: Multiracial/Native Hawaiian/Other Pacific Islander, n (%)	0 (0.0)
Race: Unknown, n (%)	7 (2.2)
Race: White, n (%)	217 (68.0)
Blood type A, n (%)	56 (17.6)
Blood type A1, n (%)	53 (16.6)
Blood type A1B, n (%)	1 (0.3)
Blood type A2, n (%)	30 (9.4)
Blood type A2B, n (%)	3 (0.9)
Blood type AB, n (%)	8 (2.5)
Blood type B, n (%)	38 (11.9)
Blood type O, n (%)	130 (40.8)
KDPI, median [IQR]	41.00 [22.50, 62.00]
DCD, n (%)	118 (37.0)
CIT 0–15 hours, n (%)	71 (22.3)
CIT 16–24 hours, n (%)	161 (50.5)
CIT $>$24 hours, n (%)	87 (27.3)
BMI, median [IQR]	27.84 [24.17, 32.71]
Terminal creatinine, median [IQR]	1.03 [0.70, 1.77]
CMV, n (%)	216 (67.7)
EBV, n (%)	182 (57.1)

E.2 ORIGINAL E3-MOFS FOR TCMR AND ABMR PREDICTION

Table 7: E3-MoFs in the patient cohort with high-resolution HLA typing.

E3-generated molecular feature (E3-MoF)	Target HLA Class I molecule	Included in TCMR- or ABMR-E3-MoFs	Median [Q1, Q3]
AML.HLA.I (median [IQR])	α_1/α_2 domain-restricted	TCMR-MoFs	45.00 [33.00, 57.00]
AML.A (median [IQR])	α_1/α_2 domain-restricted	TCMR-MoFs	16.00 [9.00, 23.00]
AML.B (median [IQR])	α_1/α_2 domain-restricted	TCMR-MoFs	17.00 [10.00, 23.00]
AML.C (median [IQR])	α_1/α_2 domain-restricted	TCMR-MoFs	10.00 [6.00, 14.00]
EML.HLA.I (median [IQR])	α_1/α_2 domain-restricted	TCMR-MoFs	80.54 [56.50, 110.84]
EML.A (median [IQR])	α_1/α_2 domain-restricted	TCMR-MoFs	30.91 [16.98, 50.25]
EML.B (median [IQR])	α_1/α_2 domain-restricted	TCMR-MoFs	25.59 [13.91, 38.08]
EML.C (median [IQR])	α_1/α_2 domain-restricted	TCMR-MoFs	19.44 [9.74, 28.12]
HML.HLA.I (median [IQR])	α_1/α_2 domain-restricted	TCMR-MoFs	89.70 [61.10, 113.25]
HML.A (median [IQR])	α_1/α_2 domain-restricted	TCMR-MoFs	32.40 [18.30, 50.05]
HML.B (median [IQR])	α_1/α_2 domain-restricted	TCMR-MoFs	30.60 [17.95, 43.75]
HML.C (median [IQR])	α_1/α_2 domain-restricted	TCMR-MoFs	20.70 [11.25, 29.75]
AML.HLA (median [IQR])	Full molecule	ABMR-MoFs	102.00 [66.00, 227.50]
AML.HLA.I (median [IQR])	Full molecule	TCMR- and ABMR-MoFs	33.00 [21.00, 43.00]
AML.A (median [IQR])	Full molecule	TCMR- and ABMR-MoFs	13.00 [7.00, 20.00]
AML.B (median [IQR])	Full molecule	TCMR- and ABMR-MoFs	9.00 [5.00, 13.00]
AML.C (median [IQR])	Full molecule	TCMR- and ABMR-MoFs	8.00 [4.00, 16.00]
AML.HLA.II (median [IQR])	Full molecule	ABMR-MoFs	64.00 [33.50, 197.00]
AML.DRB (median [IQR])	Full molecule	ABMR-MoFs	18.00 [6.00, 27.50]
AML.DRB1 (median [IQR])	Full molecule	ABMR-MoFs	8.00 [3.00, 12.00]
AML.DRB345 (median [IQR])	Full molecule	ABMR-MoFs	10.00 [0.00, 16.50]
AML.DQ (median [IQR])	Full molecule	ABMR-MoFs	18.00 [6.00, 33.00]
AML.DQA1 (median [IQR])	Full molecule	ABMR-MoFs	10.00 [2.00, 18.00]
AML.DQB1 (median [IQR])	Full molecule	ABMR-MoFs	9.00 [2.00, 16.00]
AML.DP (median [IQR])	Full molecule	ABMR-MoFs	7.00 [0.50, 172.00]
AML.DPB1 (median [IQR])	Full molecule	ABMR-MoFs	4.00 [0.00, 9.00]
AML.DPA1 (median [IQR])	Full molecule	ABMR-MoFs	0.00 [0.00, 160.00]
EML.HLA (median [IQR])	Full molecule	ABMR-MoFs	110.87 [73.09, 213.96]
EML.HLA.I (median [IQR])	Full molecule	TCMR- and ABMR-MoFs	41.79 [26.72, 57.89]
EML.A (median [IQR])	Full molecule	TCMR- and ABMR-MoFs	14.03 [5.69, 23.76]
EML.B (median [IQR])	Full molecule	TCMR- and ABMR-MoFs	9.71 [3.79, 16.80]
EML.C (median [IQR])	Full molecule	TCMR- and ABMR-MoFs	15.66 [4.24, 23.69]
EML.HLA.II (median [IQR])	Full molecule	ABMR-MoFs	59.75 [30.26, 170.20]
EML.DRB (median [IQR])	Full molecule	ABMR-MoFs	16.42 [5.56, 27.82]
EML.DRB1 (median [IQR])	Full molecule	ABMR-MoFs	7.69 [2.41, 14.45]
EML.DRB345 (median [IQR])	Full molecule	ABMR-MoFs	9.30 [0.00, 14.06]
EML.DQ (median [IQR])	Full molecule	ABMR-MoFs	17.03 [5.18, 31.92]
EML.DQA1 (median [IQR])	Full molecule	ABMR-MoFs	10.15 [1.83, 21.33]
EML.DQB1 (median [IQR])	Full molecule	ABMR-MoFs	5.68 [0.55, 11.66]
EML.DP (median [IQR])	Full molecule	ABMR-MoFs	6.05 [0.02, 136.72]
EML.DPB1 (median [IQR])	Full molecule	ABMR-MoFs	1.69 [0.00, 7.50]
EML.DPA1 (median [IQR])	Full molecule	ABMR-MoFs	0.00 [0.00, 127.91]
HML.HLA (median [IQR])	Full molecule	ABMR-MoFs	107.40 [73.20, 228.15]
HML.HLA.I (median [IQR])	Full molecule	TCMR- and ABMR-MoFs	40.60 [26.00, 55.95]
HML.A (median [IQR])	Full molecule	TCMR- and ABMR-MoFs	14.60 [6.45, 23.40]
HML.B (median [IQR])	Full molecule	TCMR- and ABMR-MoFs	10.70 [5.00, 16.95]
HML.C (median [IQR])	Full molecule	TCMR- and ABMR-MoFs	12.80 [5.05, 20.55]
HML.HLA.II (median [IQR])	Full molecule	ABMR-MoFs	59.60 [29.65, 190.80]
HML.DRB (median [IQR])	Full molecule	ABMR-MoFs	16.70 [4.95, 24.05]
HML.DRB1 (median [IQR])	Full molecule	ABMR-MoFs	5.80 [2.35, 11.20]
HML.DRB345 (median [IQR])	Full molecule	ABMR-MoFs	7.90 [0.00, 15.00]
HML.DQ (median [IQR])	Full molecule	ABMR-MoFs	16.70 [4.90, 35.75]
HML.DQA1 (median [IQR])	Full molecule	ABMR-MoFs	9.30 [1.15, 23.35]
HML.DQB1 (median [IQR])	Full molecule	ABMR-MoFs	7.30 [1.40, 15.00]
HML.DP (median [IQR])	Full molecule	ABMR-MoFs	5.00 [0.00, 159.25]
HML.DPB1 (median [IQR])	Full molecule	ABMR-MoFs	1.80 [0.00, 7.05]
HML.DPA1 (median [IQR])	Full molecule	ABMR-MoFs	0.00 [0.00, 149.80]

Table 8: E3-MoFs in the patient cohort with high-resolution HLA typing, continued.

E3-generated molecular feature (E3-MoF)	Included in TCMR- or ABMR-E3-MoFs	Median [Q1, Q3]
PC.HLA (median [IQR])	ABMR-MoFs	4.00 [1.00, 9.00]
PC.DRB (median [IQR])	ABMR-MoFs	0.00 [0.00, 0.00]
PC.DRB1 (median [IQR])	ABMR-MoFs	0.00 [0.00, 0.00]
PC.DRB345 (median [IQR])	ABMR-MoFs	0.00 [0.00, 0.00]
PC.DQ (median [IQR])	ABMR-MoFs	0.00 [0.00, 0.00]
PC.DQA (median [IQR])	ABMR-MoFs	0.00 [0.00, 0.00]
PC.DQB (median [IQR])	ABMR-MoFs	0.00 [0.00, 0.00]
PC.DP (median [IQR])	ABMR-MoFs	2.00 [0.00, 5.00]
PC.DPA (median [IQR])	ABMR-MoFs	0.00 [0.00, 0.00]
PC.DPB (median [IQR])	ABMR-MoFs	2.00 [0.00, 5.00]
EpiL.total.HLA (median [IQR])	ABMR-MoFs	75.00 [57.00, 100.00]
EpiL.reactive.HLA (median [IQR])	ABMR-MoFs	24.00 [17.00, 31.00]
EpiL.total.CI (median [IQR])	ABMR-MoFs	36.00 [25.00, 45.50]
EpiL.reactive.CI (median [IQR])	ABMR-MoFs	13.00 [8.00, 17.00]
EpiL.total.A (median [IQR])	ABMR-MoFs	14.00 [8.00, 21.00]
EpiL.reactive.A (median [IQR])	ABMR-MoFs	6.00 [3.00, 8.00]
EpiL.total.B (median [IQR])	ABMR-MoFs	11.00 [7.00, 17.00]
EpiL.reactive.B (median [IQR])	ABMR-MoFs	4.00 [2.00, 6.00]
EpiL.total.C (median [IQR])	ABMR-MoFs	8.00 [4.00, 12.00]
EpiL.reactive.C (median [IQR])	ABMR-MoFs	3.00 [1.00, 5.00]
EpiL.total.CII (median [IQR])	ABMR-MoFs	38.00 [26.00, 55.50]
EpiL.reactive.CII (median [IQR])	ABMR-MoFs	10.00 [6.00, 16.00]
EpiL.total.DRB (median [IQR])	ABMR-MoFs	18.00 [9.00, 30.50]
EpiL.reactive.DRB (median [IQR])	ABMR-MoFs	5.00 [2.00, 9.00]
EpiL.total.DRB1 (median [IQR])	ABMR-MoFs	10.00 [5.00, 15.00]
EpiL.reactive.DRB1 (median [IQR])	ABMR-MoFs	3.00 [2.00, 5.00]
EpiL.total.DRB345 (median [IQR])	ABMR-MoFs	8.00 [1.00, 15.00]
EpiL.reactive.DRB345 (median [IQR])	ABMR-MoFs	3.00 [0.00, 4.00]
EpiL.total.DQ (median [IQR])	ABMR-MoFs	12.00 [6.00, 18.00]
EpiL.reactive.DQ (median [IQR])	ABMR-MoFs	3.00 [0.00, 5.00]
EpiL.total.DQA (median [IQR])	ABMR-MoFs	4.00 [1.00, 6.00]
EpiL.reactive.DQA (median [IQR])	ABMR-MoFs	0.00 [0.00, 1.00]
EpiL.total.DQB (median [IQR])	ABMR-MoFs	8.00 [3.00, 13.00]
EpiL.reactive.DQB (median [IQR])	ABMR-MoFs	2.00 [0.00, 4.00]
EpiL.total.DP (median [IQR])	ABMR-MoFs	7.00 [1.00, 13.00]
EpiL.reactive.DP (median [IQR])	ABMR-MoFs	0.00 [0.00, 2.00]
EpiL.total.DPA (median [IQR])	ABMR-MoFs	0.00 [0.00, 5.00]
EpiL.reactive.DPA (median [IQR])	ABMR-MoFs	0.00 [0.00, 0.00]
EpiL.total.DPB (median [IQR])	ABMR-MoFs	6.00 [0.00, 10.00]
EpiL.reactive.DPB (median [IQR])	ABMR-MoFs	0.00 [0.00, 2.00]

E.3 PRINCIPAL COMPONENT ANALYSIS OF TCMR-E3-MOFS

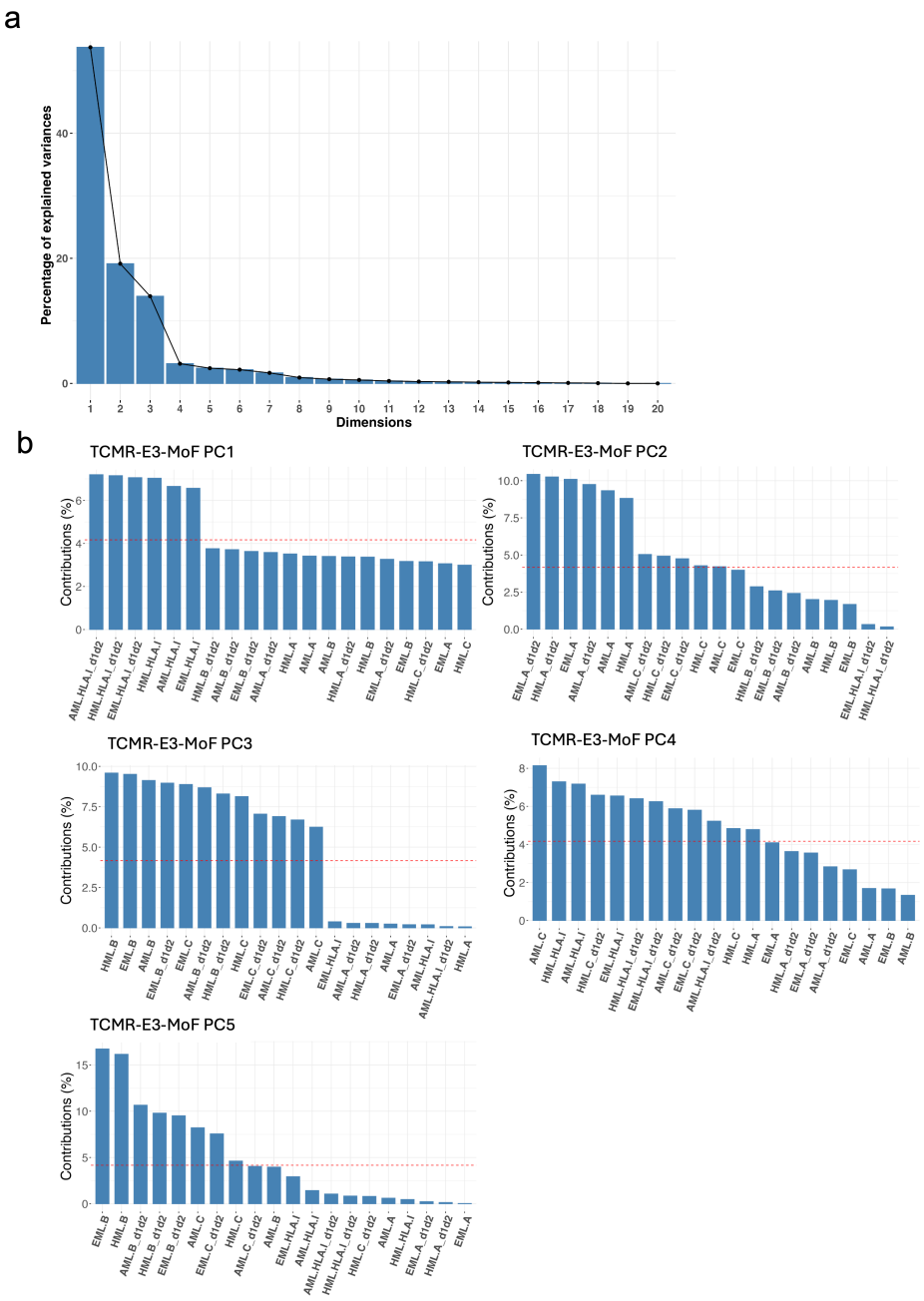

Figure 5: Principal component analysis of TCMR-E3-MoFs for the high-resolution HLA dataset. a, Screen plot showing % variance explained by each PC. b, Contributions of original molecular features to the PCs included in the models.

E.4 PRINCIPAL COMPONENT ANALYSIS OF ABMR-E3-MOFS

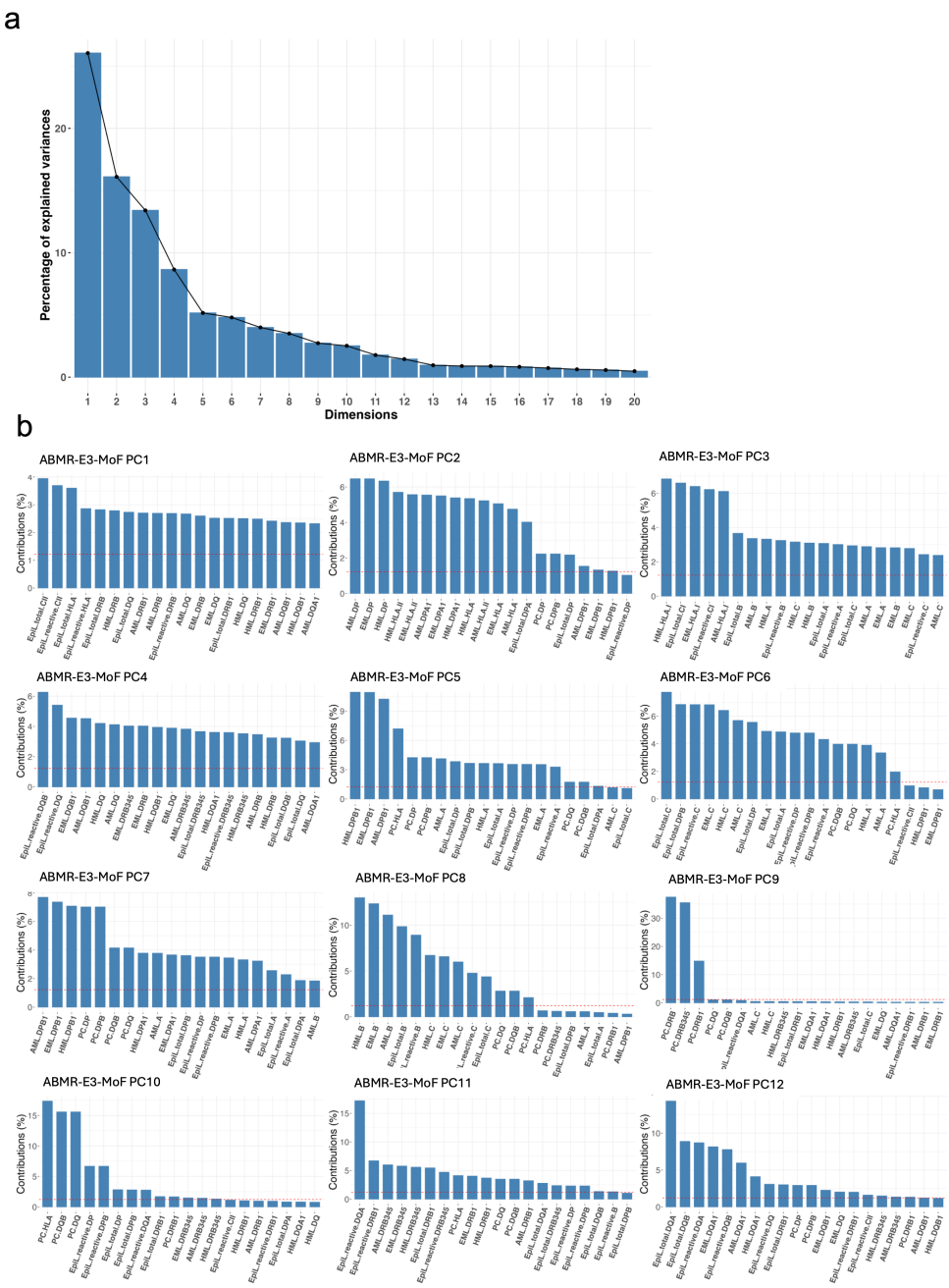

Figure 6: Principal component analysis of ABMR-E3-MoFs for the high-resolution HLA dataset. a, Screen plot showing % variance explained by each PC. b, Contributions of original molecular features to the PCs included in the models.

F MODEL CALIBRATION

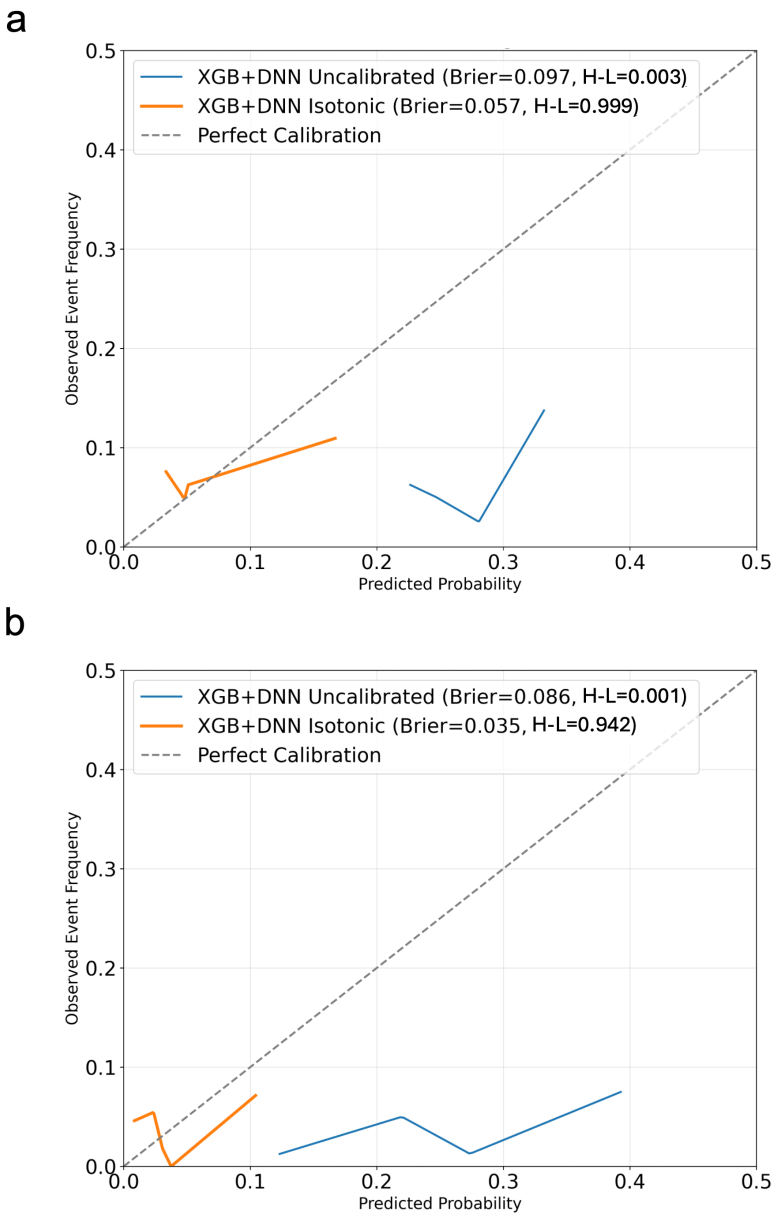

Figure 7: Calibration plots. Plots showing observed frequencies of rejection versus predicted probabilities with five bins for a, TCMR and b, ABMR. The dotted diagonal line indicates perfect calibration. Models were calibrated using isotonic regression. The Hosmer–Lemeshow (H–L) test was used to assess statistical significance.

G SHAP ANALYSIS FOR INPUT FEATURE IMPORTANCE

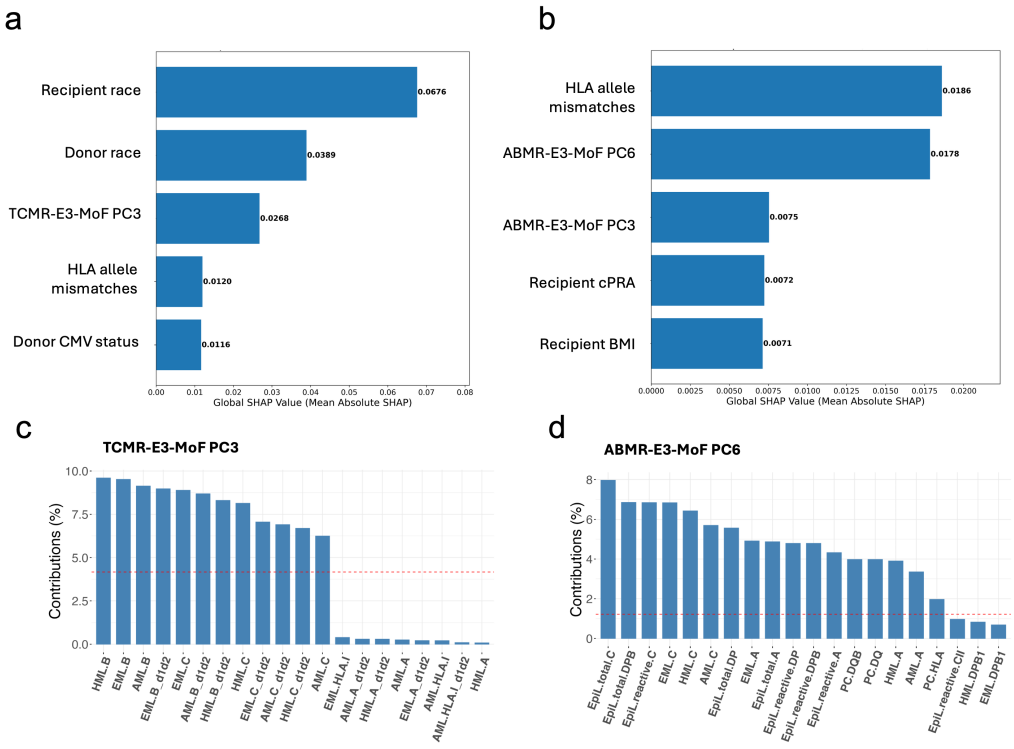

Figure 8: Input variable analysis via SHAP for the TCMR and ABMR models. Overall SHAP-derived feature importance (mean absolute SHAP values) for a, the TCMR model, and b, the ABMR model. Key contributors to the top PCs are presented, including c, TCMR-E3-MoF PC3 d, ABMR-E3-MoF PC6.

H PROSPECTIVE VALIDATION COHORT

H.1 PATIENT DEMOGRAPHICS

Table 9: Demographic and clinical characteristics of the prospective validation cohort with high-resolution HLA typing.

Characteristic	Prospective validation cohort ($n = 82$)
Recipient characteristics	
Male, n (%)	55 (67.1)
Age, median [IQR]	57.00 [47.00, 63.75]
Non-Hispanic/Latino, n (%)	63 (76.8)
Race: Amer Ind/Alaska Native, n (%)	5 (6.1)
Race: Asian, n (%)	6 (7.3)
Race: Black, n (%)	22 (26.8)
Race: Hispanic, n (%)	16 (19.5)
Race: Multiracial/Native Hawaiian/Other Pacific Islander, n (%)	3 (3.7)
Race: White, n (%)	30 (36.6)
Race: Unknown/choose not to disclose, n (%)	0 (0.0)
Pre-transplant diabetes, n (%)	36 (43.9)
Previous kidney transplant, n (%)	12 (14.6)
Pretransplant dialysis, n (%)	74 (90.2)
BMI at transplant, median [IQR]	29.03 [24.02, 33.25]
cPRA, median [IQR]	0.00 [0.00, 24.50]
Days on waitlist, median [IQR]	1102.00 [505.50, 2054.75]
CMV, n (%)	49 (59.8)
EBV, n (%)	81 (98.8)
CMV mismatch, n (%)	42 (51.2)
EBV mismatch, n (%)	29 (35.4)
Blood type A, n (%)	24 (29.3)
Blood type AB, n (%)	2 (2.4)
Blood type B, n (%)	17 (20.7)
Blood type O, n (%)	39 (47.6)
HLA mismatch, median [IQR]	13.00 [11.00, 14.00]
Induction therapy: Thymoglobulin, n (%)	20 (24.4)
Induction therapy: Simulect, n (%)	26 (31.7)
Induction therapy: Campath, n (%)	36 (43.9)
1-year TCMR, n (%)	4 (4.9)
1-year ABMR, n (%)	3 (3.7)
Donor characteristics	
Age, median [IQR]	40.00 [34.00, 51.00]
Non-Hispanic/Latino, n (%)	67 (81.7)
Race: Amer Ind/Alaska Native, n (%)	1 (1.2)
Race: Asian, n (%)	0 (0.0)
Race: Black, n (%)	4 (4.9)
Race: Hispanic, n (%)	10 (12.2)
Race: Multiracial/Native Hawaiian/Other Pacific Islander, n (%)	1 (1.2)
Race: Unknown, n (%)	3 (3.7)
Race: White, n (%)	63 (76.8)
Blood type A, n (%)	9 (11.0)
Blood type A1, n (%)	13 (15.9)
Blood type A1B, n (%)	0 (0.0)
Blood type A2, n (%)	11 (13.4)
Blood type A2B, n (%)	1 (1.2)
Blood type AB, n (%)	0 (0.0)
Blood type B, n (%)	9 (11.0)
Blood type O, n (%)	39 (47.6)
KDPI, median [IQR]	46.00 [27.25, 65.50]
DCD, n (%)	34 (41.5)
CIT 0–15 hours, n (%)	16 (19.5)
CIT 16–24 hours, n (%)	43 (52.4)
CIT >24 hours, n (%)	23 (28.0)
BMI, median [IQR]	27.00 [24.39, 31.98]
Terminal creatinine, median [IQR]	1.00 [0.69, 2.72]
CMV, n (%)	47 (57.3)
EBV, n (%)	54 (65.9)

H.2 ORIGINAL E3-MOFS FOR TCMR AND ABMR PREDICTION

Table 10: E3-MoFs in the prospective validation cohort with high-resolution HLA typing.

E3-generated molecular feature (E3-MoF)	Target HLA Class I molecule	Included in TCMR- or ABMR-E3-MoFs	Median [Q1, Q3]
AML.HLA.I (median [IQR])	α_1/α_2 domain-restricted	TCMR-MoFs	45.00 [35.00, 59.00]
AML.A (median [IQR])	α_1/α_2 domain-restricted	TCMR-MoFs	16.00 [9.00, 23.50]
AML.B (median [IQR])	α_1/α_2 domain-restricted	TCMR-MoFs	18.00 [12.25, 24.00]
AML.C (median [IQR])	α_1/α_2 domain-restricted	TCMR-MoFs	9.50 [6.00, 15.00]
EML.HLA.I (median [IQR])	α_1/α_2 domain-restricted	TCMR-MoFs	82.34 [56.66, 110.43]
EML.A (median [IQR])	α_1/α_2 domain-restricted	TCMR-MoFs	28.87 [14.48, 48.84]
EML.B (median [IQR])	α_1/α_2 domain-restricted	TCMR-MoFs	26.18 [18.18, 38.08]
EML.C (median [IQR])	α_1/α_2 domain-restricted	TCMR-MoFs	19.58 [10.02, 32.46]
HML.HLA.I (median [IQR])	α_1/α_2 domain-restricted	TCMR-MoFs	91.85 [66.88, 115.40]
HML.A (median [IQR])	α_1/α_2 domain-restricted	TCMR-MoFs	32.80 [15.65, 50.75]
HML.B (median [IQR])	α_1/α_2 domain-restricted	TCMR-MoFs	31.40 [22.00, 47.52]
HML.C (median [IQR])	α_1/α_2 domain-restricted	TCMR-MoFs	19.70 [11.95, 34.32]
AML.HLA (median [IQR])	Full molecule	ABMR-MoFs	138.50 [83.25, 265.00]
AML.HLA.I (median [IQR])	Full molecule	TCMR- and ABMR-MoFs	34.00 [24.00, 46.00]
AML.A (median [IQR])	Full molecule	TCMR- and ABMR-MoFs	12.00 [7.00, 18.75]
AML.B (median [IQR])	Full molecule	TCMR- and ABMR-MoFs	9.50 [6.00, 13.75]
AML.C (median [IQR])	Full molecule	TCMR- and ABMR-MoFs	8.00 [4.00, 17.75]
AML.HLA.II (median [IQR])	Full molecule	ABMR-MoFs	85.00 [41.25, 222.50]
AML.DRB (median [IQR])	Full molecule	ABMR-MoFs	18.00 [6.25, 30.00]
AML.DRB1 (median [IQR])	Full molecule	ABMR-MoFs	8.00 [4.00, 14.00]
AML.DRB345 (median [IQR])	Full molecule	ABMR-MoFs	10.00 [0.00, 17.75]
AML.DQ (median [IQR])	Full molecule	ABMR-MoFs	19.00 [8.00, 35.50]
AML.DQA1 (median [IQR])	Full molecule	ABMR-MoFs	8.50 [2.00, 20.00]
AML.DQB1 (median [IQR])	Full molecule	ABMR-MoFs	10.50 [4.00, 16.00]
AML.DP (median [IQR])	Full molecule	ABMR-MoFs	8.50 [2.25, 185.50]
AML.DPB1 (median [IQR])	Full molecule	ABMR-MoFs	7.50 [1.00, 12.00]
AML.DPA1 (median [IQR])	Full molecule	ABMR-MoFs	1.00 [0.00, 164.00]
EML.HLA (median [IQR])	Full molecule	ABMR-MoFs	135.20 [87.88, 274.91]
EML.HLA.I (median [IQR])	Full molecule	TCMR- and ABMR-MoFs	43.15 [30.02, 54.39]
EML.A (median [IQR])	Full molecule	TCMR- and ABMR-MoFs	12.63 [3.76, 22.32]
EML.B (median [IQR])	Full molecule	TCMR- and ABMR-MoFs	10.32 [5.54, 14.97]
EML.C (median [IQR])	Full molecule	TCMR- and ABMR-MoFs	17.24 [4.60, 27.57]
EML.HLA.II (median [IQR])	Full molecule	ABMR-MoFs	86.88 [35.86, 247.30]
EML.DRB (median [IQR])	Full molecule	ABMR-MoFs	17.93 [7.41, 27.65]
EML.DRB1 (median [IQR])	Full molecule	ABMR-MoFs	7.93 [3.76, 13.01]
EML.DRB345 (median [IQR])	Full molecule	ABMR-MoFs	10.02 [0.00, 13.20]
EML.DQ (median [IQR])	Full molecule	ABMR-MoFs	15.17 [6.96, 32.49]
EML.DQA1 (median [IQR])	Full molecule	ABMR-MoFs	9.04 [2.43, 20.98]
EML.DQB1 (median [IQR])	Full molecule	ABMR-MoFs	6.63 [1.23, 12.54]
EML.DP (median [IQR])	Full molecule	ABMR-MoFs	14.04 [0.29, 158.36]
EML.DPB1 (median [IQR])	Full molecule	ABMR-MoFs	2.45 [0.13, 12.96]
EML.DPA1 (median [IQR])	Full molecule	ABMR-MoFs	0.11 [0.00, 138.86]
HML.HLA (median [IQR])	Full molecule	ABMR-MoFs	142.45 [84.62, 310.90]
HML.HLA.I (median [IQR])	Full molecule	TCMR- and ABMR-MoFs	41.90 [26.80, 55.27]
HML.A (median [IQR])	Full molecule	TCMR- and ABMR-MoFs	13.45 [5.90, 22.25]
HML.B (median [IQR])	Full molecule	TCMR- and ABMR-MoFs	10.65 [5.95, 17.60]
HML.C (median [IQR])	Full molecule	TCMR- and ABMR-MoFs	14.75 [6.28, 24.80]
HML.HLA.II (median [IQR])	Full molecule	ABMR-MoFs	97.20 [34.75, 265.45]
HML.DRB (median [IQR])	Full molecule	ABMR-MoFs	17.95 [6.53, 27.35]
HML.DRB1 (median [IQR])	Full molecule	ABMR-MoFs	6.35 [3.42, 12.95]
HML.DRB345 (median [IQR])	Full molecule	ABMR-MoFs	8.00 [0.00, 15.23]
HML.DQ (median [IQR])	Full molecule	ABMR-MoFs	14.70 [7.73, 37.25]
HML.DQA1 (median [IQR])	Full molecule	ABMR-MoFs	6.05 [1.72, 22.75]
HML.DQB1 (median [IQR])	Full molecule	ABMR-MoFs	8.30 [3.05, 14.42]
HML.DP (median [IQR])	Full molecule	ABMR-MoFs	7.05 [0.50, 176.52]
HML.DPB1 (median [IQR])	Full molecule	ABMR-MoFs	3.75 [0.20, 9.07]
HML.DPA1 (median [IQR])	Full molecule	ABMR-MoFs	0.40 [0.00, 163.50]

Table 11: E3-MoFs in the prospective validation cohort with high-resolution HLA typing, continued.

E3-generated molecular feature (E3-MoF)	Included in TCMR- or ABMR-E3-MoFs	Median [Q1, Q3]
PC.HLA (median [IQR])	ABMR-MoFs	3.50 [2.00, 8.00]
PC.DRB (median [IQR])	ABMR-MoFs	0.00 [0.00, 0.00]
PC.DRB1 (median [IQR])	ABMR-MoFs	0.00 [0.00, 0.00]
PC.DRB345 (median [IQR])	ABMR-MoFs	0.00 [0.00, 0.00]
PC.DQ (median [IQR])	ABMR-MoFs	0.00 [0.00, 0.00]
PC.DQA (median [IQR])	ABMR-MoFs	0.00 [0.00, 0.00]
PC.DQB (median [IQR])	ABMR-MoFs	0.00 [0.00, 0.00]
PC.DP (median [IQR])	ABMR-MoFs	2.00 [0.00, 4.75]
PC.DPA (median [IQR])	ABMR-MoFs	0.00 [0.00, 0.00]
PC.DPB (median [IQR])	ABMR-MoFs	2.00 [0.00, 4.75]
EpiL.total.HLA (median [IQR])	ABMR-MoFs	81.00 [67.50, 98.75]
EpiL.reactive.HLA (median [IQR])	ABMR-MoFs	26.50 [19.25, 31.00]
EpiL.total.CI (median [IQR])	ABMR-MoFs	33.50 [25.50, 48.00]
EpiL.reactive.CI (median [IQR])	ABMR-MoFs	12.50 [9.00, 18.75]
EpiL.total.A (median [IQR])	ABMR-MoFs	13.50 [7.00, 20.00]
EpiL.reactive.A (median [IQR])	ABMR-MoFs	5.00 [2.00, 9.00]
EpiL.total.B (median [IQR])	ABMR-MoFs	13.50 [9.00, 19.00]
EpiL.reactive.B (median [IQR])	ABMR-MoFs	5.00 [3.00, 6.00]
EpiL.total.C (median [IQR])	ABMR-MoFs	8.00 [4.00, 12.75]
EpiL.reactive.C (median [IQR])	ABMR-MoFs	3.00 [1.25, 4.00]
EpiL.total.CII (median [IQR])	ABMR-MoFs	46.00 [28.00, 56.75]
EpiL.reactive.CII (median [IQR])	ABMR-MoFs	13.00 [7.00, 17.00]
EpiL.total.DRB (median [IQR])	ABMR-MoFs	20.00 [9.25, 28.75]
EpiL.reactive.DRB (median [IQR])	ABMR-MoFs	6.00 [3.25, 8.75]
EpiL.total.DRB1 (median [IQR])	ABMR-MoFs	10.50 [6.00, 16.00]
EpiL.reactive.DRB1 (median [IQR])	ABMR-MoFs	4.00 [2.00, 5.00]
EpiL.total.DRB345 (median [IQR])	ABMR-MoFs	8.50 [0.00, 14.00]
EpiL.reactive.DRB345 (median [IQR])	ABMR-MoFs	3.00 [0.00, 4.00]
EpiL.total.DQ (median [IQR])	ABMR-MoFs	13.00 [6.25, 18.00]
EpiL.reactive.DQ (median [IQR])	ABMR-MoFs	3.50 [1.00, 6.50]
EpiL.total.DQA (median [IQR])	ABMR-MoFs	3.00 [1.00, 5.00]
EpiL.reactive.DQA (median [IQR])	ABMR-MoFs	0.00 [0.00, 1.00]
EpiL.total.DQB (median [IQR])	ABMR-MoFs	9.50 [5.00, 13.00]
EpiL.reactive.DQB (median [IQR])	ABMR-MoFs	2.50 [0.00, 5.00]
EpiL.total.DP (median [IQR])	ABMR-MoFs	8.00 [4.00, 17.75]
EpiL.reactive.DP (median [IQR])	ABMR-MoFs	1.00 [0.00, 3.00]
EpiL.total.DPA (median [IQR])	ABMR-MoFs	0.00 [0.00, 5.00]
EpiL.reactive.DPA (median [IQR])	ABMR-MoFs	0.00 [0.00, 0.00]
EpiL.total.DPB (median [IQR])	ABMR-MoFs	6.00 [1.00, 12.00]
EpiL.reactive.DPB (median [IQR])	ABMR-MoFs	1.00 [0.00, 3.00]